

THE LUMINOSITY FUNCTION AND INITIAL MASS FUNCTION IN THE GALACTIC BULGE ¹

Jon A. Holtzman², Alan M. Watson³, William A. Baum⁴, Carl J. Grillmair⁵,
Edward J. Groth⁶, Robert M. Light⁷, Roger Lynds⁸, Earl J. O'Neil, Jr.⁸

ABSTRACT

We present deep photometry obtained with the Hubble Space Telescope (HST) in a field in Baade's Window in the Galactic bulge. We derive a luminosity function down to $I \sim 24.3$, or $V \sim 27.5$, corresponding to $M \sim 0.3M_{\odot}$. The luminosity function from the turnoff down to this level appears remarkably similar to that observed in the solar neighborhood. We derive a mass function using both an empirical local mass-luminosity relation and a mass-luminosity relation from recent stellar model calculations, allowing for the presence of binaries and photometric errors. The mass function has a power law form with $dN/dM \propto M^{-2.2}$ for $M \gtrsim 0.7M_{\odot}$. However, we find strong evidence for a break in the mass function slope around 0.5-0.7 M_{\odot} , with a significantly shallower slope at lower masses. The value of the slope for the low masses depends on the assumed binary fraction and the accuracy of our completeness correction. This mass function should directly reflect the *initial* mass function.

¹Based on observations with the NASA/ESA *Hubble Space Telescope*, obtained at the Space Telescope Science Institute, operated by AURA Inc under contract to NASA

²Department of Astronomy, New Mexico State University, Dept 4500 Box 30001, Las Cruces, NM 88003, holtz@nmsu.edu, awatson@nmsu.edu

³Instituto de Astronomía UNAM, J. J. Tablada 1006, Col. Lomas de Santa Maria, 58090 Morelia, Michoacán, Mexico, alan@astrosmo.unam.mx

⁴Astronomy Department, University of Washington, Seattle WA 98195, baum@astro.washington.edu

⁵Jet Propulsion Laboratory, 4800 Oak Grove Drive, Pasadena, CA 91109, carl@wfp2-mail

⁶Department of Physics, Princeton University, Princeton, NJ 08544, groth@pupgg.princeton.edu

⁷Caltech/IPAC, MS 100-22, Pasadena, CA 91125, light@ipac.caltech.edu

⁸Kitt Peak National Observatory, Box 26732, Tucson AZ 85726, lynds@noao.edu, oneil@noao.edu

1. Introduction

The luminosity function of low mass stars is particularly interesting because it can be used to infer the initial mass function (IMF) independently of the star formation history, since low mass stars evolve relatively little over the entire lifetime of the Universe. Understanding whether or not there are variations of the IMF with galaxy type or with metallicity is essential to our understanding of star formation and to the modelling of galaxy evolution. To date, most observations of IMFs of low mass stars have been made, by necessity, in nearby systems.

In the solar neighborhood, estimates of the low-mass IMF have been made by Salpeter (1955), Miller & Scalo (1979), and Kroupa, Tout, & Gilmore (1993) (among others). The latter find that a segmented power law, $dN/dM \propto M^\alpha$ best represents the local IMF, with $\alpha = -2.7$ for $M > 1M_\odot$, $\alpha = -2.2$ for $0.5 < M < 1M_\odot$, and $-1.85 < \alpha < -0.7$ for $M < 0.5M_\odot$. The mass function of the least massive stars is of particular interest in connection with the frequency of brown dwarfs, the local mass density in the Galactic disk, and the observed microlensing rates towards the LMC and the Galactic bulge. Other recent studies of the local neighborhood also find a flattening of the IMF slope at low masses; Gould, Bahcall, & Flynn (1997) find $\alpha = -0.56$ for $M < 0.5M_\odot$ for HST observations of local M dwarfs. The Gould et al. slope does not include a correction for the presence of binaries; allowing for these brings the inferred slope into the range suggested by Kroupa et al. (1993), who did make a correction for binaries.

Measurements of the luminosity and mass functions in the Galactic halo have been recently reviewed by Mould (1996); conflicting results have been reported. Dahn et al. (1995) find a turnover in the halo luminosity function, while Richer & Fahlman (1992) find evidence for a rapidly increasing number of stars as one goes to lower masses. In support of the Dahn et al. result, Gould, Flynn, & Bahcall (1997) derive a mass function with a shallow slope of $\alpha \sim -0.75$ from analysis of 166 spheroid subdwarfs observed with HST.

Other estimates of IMFs have been made in stellar clusters and associations, both in the Galaxy and in some nearby stellar systems. Most of these measurements suggest IMFs similar to those observed in the solar neighborhood, although there are some exceptions; Hunter et al. (1997) present a recent summary. However, measurements of stars with $M < 0.5M_\odot$ have been difficult to make. DeMarchi & Paresce (1995a, 1995b, 1997) have measured the luminosity function down to very low mass stars in several nearby globular clusters using HST, and they find an increasing number of stars with decreasing mass down to $\sim 0.2 M_\odot$, but then a flattening of the luminosity function towards lower masses. However, this is in conflict with previous ground-based measurements in these clusters, which suggest steeply rising mass functions down to the lowest mass stars observed (Richer

et al. 1991). In general, the connection between current cluster mass functions and their initial mass function may be complicated because of dynamical evolution within a cluster and the removal of stars by the tidal field of the parent galaxy.

In nearby galaxies, the ability of HST to observe individual faint stars has allowed estimates of the initial mass function down to relatively low stellar masses ($M \sim 0.7 M_{\odot}$). However, the conversion between a luminosity function and a mass function is not totally independent of the star formation history for such stars because these stars evolve in luminosity in less than a Hubble time. In an outer field in the Large Magellanic Cloud (LMC), Holtzman et al. (1997) find that a solar neighborhood initial mass function provides an adequate match to the data, but only if there is a significant component of older stars in the LMC. If the stars in the LMC field are predominantly young, then a steeper IMF, with $\alpha \sim -2.75$, is required. In the nearby dwarf spheroidal Draco, the inferred IMF is similarly linked to the age of the system (Grillmair et al. 1998); for an age of 12 Gyr, the inferred IMF slope is comparable to that of the solar neighborhood.

Consequently, a picture is emerging which suggests, remarkably, that the initial mass function does not appear to vary significantly from one environment to another. However, much of the interpretation is still complicated by lack of knowledge about star formation histories, which affect inferences about the initial mass function for all except very low mass stars, and by the possible effects of dynamical evolution in star clusters. Additionally, initial mass functions have not been measured for all types of stellar systems. In particular, no metal-rich systems have been studied, nor have any massive spheroidal systems.

A determination of the initial mass function of the Galactic bulge for comparison with that of the disk is important because of the possibility of differing modes of star formation in spheroidal and disk systems. Furthermore, a measurement of the mass function of stars in the bulge is essential to interpretations of microlensing events observed in the direction of the Galactic center (e.g., Alcock et al. 1997).

We have observed a field in Baade’s Window with the Wide Field Planetary Camera 2 on the Hubble Space Telescope in order to observe faint, low mass, stars. Our observations probe to stars with $M \sim 0.25 M_{\odot}$. In this paper we concentrate on the luminosity function of the faint stars, and its implications for the mass function in the bulge. A subsequent paper will discuss the interpretation of the color-magnitude diagram in greater detail, concentrating on what it can tell us about the star formation history in the Galactic bulge.

2. Observations

Observations of Baade’s Window were obtained on 12 August 1994 with the Wide Field Planetary Camera 2 of the Hubble Space Telescope. Observations were made through the F555W and F814W filters (wide V and I) with a total of 2420s through each filter. Observations through each filter were split into 5 exposures with exposure times of 20, 200, 200, 1000, and 1000 seconds. To maximize the dynamic range, the short exposures were made with a gain of ~ 14 electrons/DN, and the long exposures were made with gain ~ 7 electrons/DN.

The data were processed using the standard reduction techniques discussed by Holtzman et al. (1995a, H95A). This processing included a very small correction for analog-to-digital errors, overscan and bias subtraction, dark subtraction, a tiny shutter shading correction, and flat fielding.

2.1. Photometry

Figure 1 shows the combined set of F555W exposures. The field is crowded and profile-fitting photometry is required to get accurate results for the faint stars.

To perform the profile-fitting photometry, the five frames in each color were first combined to reject cosmic rays based on the known noise properties of the WFPC2 detectors. Since the F814W frames were deeper (because we are probing to low mass, very red stars), star detection was performed on the F814W frame alone. Given the input star list, profile fitting was performed simultaneously on the set of ten individual frames, solving for a brightness for each star in each color, a position for each star, a separate background value for each group of stars in each frame, and frame-to-frame pointing shifts. Simultaneous fitting imposes the requirement that all frames have the same star list with the same relative positions (after allowing for the variation in scale as a function of wavelength as discussed in H95A). Small pointing differences between the frames provide slightly different pixel samplings of the PSF, providing additional information for fitting the undersampled PSF. Model PSFs that vary across the field of view were used; separate models were derived for each of the individual frames allowing for small focus shifts between frames. A brief description of the model PSFs and their advantages and disadvantages is presented in Holtzman et al. (1997). Cosmic rays in each of the individual frames were flagged by the procedure which combined the stack of frames for star-finding, and contaminated pixels were ignored in the profile-fitting procedure.

Because of the large range in luminosities of stars observed in the bulge, the wings

of the bright stars cause significant problems for automatic star finding algorithms. To minimize the problem, the profile fitting was iterated three times. In the first pass, only the brightest stars were fit. This allowed identification and subtraction of these stars including the extensive stellar wings and diffraction spikes. In the second pass, the star finding algorithm was used on the subtracted frames, with a low threshold to detect faint stars. A higher detection threshold was used around bright stars in the subtracted frame to avoid spurious detections from imperfect PSF subtraction. A fit was then performed on the original frames including stars found on both first and second passes, and these stars were subtracted. In the third pass, a few additional close neighbors of stars were detected from these subtracted frames. These were added to the list of stars, and a final stellar photometry run was made. During each of the profile-fitting stages, the software attempted to remove spurious detections by deleting stars that were not well fit by the stellar PSF. The final photometry list was filtered once again using a goodness-of-fit index in an attempt to remove spurious detections which remained.

The resulting magnitudes were placed on the synthetic WFPC2 photometric system defined by Holtzman et al. (1995b, hereafter H95B). The profile results were converted to instrumental aperture magnitudes with a 0.5 arcsec radius aperture using aperture photometry of reasonably bright stars after subtraction of their neighbors based on the profile fitting results. The aperture corrections were determined by inspecting the difference between the 0.5 arcsec aperture and profile-fitting results; a separate correction was determined for each of the four chips, although they all agreed to within a few percent. We judge the accuracy of the aperture corrections to be a few percent in the worst case. Because these were fairly long, crowded exposures, we made no correction for possible errors from charge transfer efficiency (CTE) effects, as discussed in H95B; if CTE problems were present they would only change the derived magnitudes by a few percent and our conclusions would be unaffected. No correction was made for a possible systematic effect which may give differences in photometric zeropoint between long and short exposures (see Note Added in Proof, H95B); applying such a correction would make all our magnitudes about 0.05 mag fainter, which would also have a minimal impact on our conclusions.

To compare with local luminosity functions which have been derived in the V and I bandpasses, we also transformed our WFPC2 magnitudes to the Johnson/Cousins VI system using the synthetic transformations presented in H95B. These transformations were derived from a stellar library which included stars as red as those observed here. The use of these transformations introduces some potential systematic errors because of the unknown metallicity dependence of the transformations, but such errors are likely to be small. In any case, most of the work presented below is performed in the native WFPC2 system.

The calibrated color-magnitude diagrams (with both F555W and F814W on the ordinate) are presented in Figure 2. A well defined main sequence can be seen down to $F555W \sim V > 27$.

2.2. Completeness and Error Estimation

To accurately interpret the luminosity function, we need to understand the detection efficiency and measurement errors as a function of stellar brightness. To estimate these, we performed a series of artificial star experiments in which we added a grid of stars of equal brightness onto each exposure in each of the four chips. Artificial stars were given colors corresponding to the median color of observed stars at a comparable magnitude, so fainter stars were made to be redder. The grid spacings were chosen to insure that the artificial stars were isolated from each other and thus did not add significantly to the crowding on the frame; 529 stars were placed on each of the WFs, and 121 were placed on the PC. Different pixel centerings were used for each artificial star, and the pixel centering varied slightly from frame-to-frame as in the real data. Poisson statistics were used to add errors to the artificial stars. These frames were then run through photometry routines identical to those discussed in Section 2.1. This was done 22 separate times with different brightnesses chosen for the artificial stars each time.

For each of the artificial star runs, the final list from the photometry procedure was compared with the input list of artificial stars, and also with the final photometry list from the original frames. An artificial star was considered to be found if there was a detection within one pixel of the position where the star was placed and if there was no corresponding detection on the original frame. If a match was found with both the artificial star position and with an object on the original frame, the artificial star was considered found if the measured F555W magnitude was closer to the magnitude of the artificial star than to the magnitude of the star on the original frames. This properly accounts for incompleteness arising from crowding as well as from incompleteness from inability to detect stars in the noise of the background.

The artificial stars also provided an estimate of the photometric errors, at least for the fainter stars. A limitation is that the artificial stars are created and measured with the same PSF, so there are no errors resulting from inaccuracies in the PSF models. Such errors dominate for brighter stars, so the artificial stars cannot be used to judge the photometric errors for these stars. Errors in the fainter stars are dominated by photon statistics and include both random and systematic errors. The former comes from Poisson statistics and readout noise, but systematic errors also occur at the faintest levels because objects with

positive noise fluctuations are detected preferentially over those with negative fluctuations. Systematic errors can also arise from crowding.

Some of the measured completeness and error distributions for the F814W magnitudes are shown in Figure 3. Each panel shows a histogram of observed errors for artificial stars of a different brightness. The text in each panel identifies the artificial star brightness (F555W and F814W) as well as the completeness fraction (fraction of artificial stars detected and measured). As expected, the random error increases for fainter objects. In addition, for the faintest objects, it is clear that the error distribution is asymmetric for the F814W magnitudes, with more stars being detected too bright than too faint. This is expected, since the faintest objects may only be detected if they have a positive noise fluctuation. Crowding may also contribute to this result.

The accuracy of the completeness tests is different for the two different filters, because star detection is performed only on the F814W frames. The probability that an artificial star will be detected depends on its F814W magnitude. Consequently, completeness as a function of input F814W magnitude is accurately measured, but completeness as a function of input F555W magnitude is accurate only to the extent to which the artificial stars have the *same color* as the true stars. The artificial star colors were chosen based on median colors of the observed real stars, but these are likely to be biased for the faintest stars by incompleteness. Consequently, we believe that the F814W corrected luminosity function is more accurate than the corresponding function in F555W. In addition, random errors are smaller in F814W for the faintest stars, so smearing of the luminosity function from observational error is smaller in the F814W luminosity function.

We have attempted to assess possible errors in our completeness corrections by repeating the test with simulated stars made using a PSF that has a severely different focus from that inferred from the actual frames. We then reduced these frames with our normal PSFs to simulate the effect of using an erroneous PSF. Completeness results for the two different PSFs are shown in Figure 4. Although these differ significantly for the faint objects, we note that in the repeat test we used a PSF for the fake objects which was an extreme mismatch; the subtractions from our incorrect PSFs were glaring and far worse than any subtractions of comparably bright real stars. Consequently, we feel that the differences illustrated between these two completeness curves represent the extreme of possible errors.

Spurious detections are more problematic than missed detections, since it is more difficult to estimate their frequency. We have attempted to minimize the number of spurious detections by using a relatively high star finding threshold, and by using a conservative limit on goodness-of-fit for accepting objects for which we perform photometry. Visual

inspection shows that we do not appear to have a large number of spurious detections remaining after these techniques are applied; in subsequent analysis, we make no effort to correct for the few which have survived, since we cannot determine a reasonable estimate for the number of spurious detections as a function of apparent magnitude.

3. Interpretation

3.1. Distance and reddening

We have adopted a distance of 8 kpc for the bulge (see, e.g., Carney et al. 1995), with a corresponding distance modulus of 14.52. Maximum errors in this are probably about 0.3 mag (corresponding to distances between 7 and 9 kpc). Of course, the bulge population sampled is likely to lie at a range of distances, causing the observed luminosity function to be smeared.

The extinction in the direction of Baade’s Window has been discussed by Stanek (1996), Gould, Popowski, & Terndrup (1998), and Alcock et al. (1998), among others. Stanek (1996) presents a map of differential reddening within Baade’s Window based on brightnesses of red clump stars. Gould et al. (1998) have computed a zero point for this map based on observed $(V - K)$ colors as compared with $(V - K)_0$ predicted from observed $H\beta$ indices. Alcock et al. (1998) independently compute a zeropoint based on observations of RR Lyrae stars and derive an almost identical zeropoint to that of Gould et al. Using this zeropoint and the Stanek map, we infer an extinction of $A_V = 1.28 \pm 0.08$ for our field, which lies in one of the clearest regions of Baade’s Window. Using the calculations of Holtzman et al. (1995b), we infer extinctions in the WFPC2 filters system of $A(F555W) = 1.26$ and $A(F814W) = 0.76$.

3.2. The luminosity function

Figure 5 shows the observed luminosity function in the V and I bands. Both the uncorrected (open squares) and completeness-corrected (filled squares) luminosity functions are shown. The completeness correction here uses the completeness fraction as measured from simulated stars of the corresponding magnitude. The application of the completeness correction in this way is only approximate because it assumes that stars are measured without observational error; in reality, stars observed at a given magnitude actually have a range of true magnitudes, and, correspondingly, different detection probabilities. However, random errors are not likely to have much effect because the luminosity function is relatively

flat, and, as shown above, systematic errors are not important until $V \sim 28$, or $M_V \sim 12$. Similarly, spread in the distance of the stars is not likely to significantly affect the relatively flat luminosity function.

We show the corrected luminosity function for $M_V < 12.25$ and $M_I < 9$; as discussed above, the completeness correction for I is probably more reliable than that for V because the latter depends on the accuracy of the simulated star colors. Errors in the completeness correction are a likely cause of the apparent turnover in the V band luminosity function at the faintest magnitudes. For the I band, we expect that the error in completeness gives an uncertainty of $\lesssim 50\%$ in the counts at the very faintest magnitude shown.

For comparison, we also show the solar neighborhood luminosity function from Wielen et al. (1983) (triangles), as well as a recent determination of the local luminosity function for M dwarfs as derived by HST imaging (asterisks, Gould et al. 1997). The luminosity functions have been normalized to agree at $M_V = 9$ and $M_I = 7.25$. For the I band, these luminosity functions have been transformed from the V band using the relation between V and $V - I$ presented by Kroupa & Tout (1997) based on the data of Monet et al (1992).

It is immediately apparent that the corrected bulge luminosity function is in close agreement with the solar neighborhood luminosity function over the range $7 < M_V < 11$ and $6 < M_I < 9$. Brighter than this, the bulge luminosity function drops off more steeply than the local function, as expected for an older population. The one discrepant point from the Gould et al. luminosity function ($M_V \sim 8.3$) has a large associated error because few stars this bright are counted in the HST fields.

However, the match of the luminosity function with that of the solar neighborhood does not necessarily imply a correspondence in the mass functions because of possible differences in the number of binaries in the samples and because of observational errors. To consider these effects, we turn to a discussion of the inferred mass function.

3.3. The mass-luminosity relation

The IMF is constrained using the lower main sequence because the effects of stellar evolution are minimal for low mass stars over the age of the universe. However, the derived mass function depends on an accurate knowledge of the mass-luminosity relation, and calculations indicate that the mass-luminosity relation depends on metallicity (Kroupa & Tout 1997). Theoretical mass-luminosity relations are difficult to calculate for low mass stars because of complications from the equation of state, opacities, and convection, leading to uncertainties in the mass-luminosity relation as derived from models. However, recent

progress has been made by Baraffe et al. (1997). These models incorporate the most up-to-date physics available and are computed self-consistently with the stellar atmospheres of Allard et al. (1997). So far, we have obtained these models only for stars up to $0.7 M_{\odot}$; for more massive stars (which do not enter strongly into the discussion in this paper), we have used models from the Padua group (Bertelli et al. 1994; Bressan et al. 1993; Fagotto et al. 1994a,b). A good summary of the current understanding of mass-luminosity relations is presented by Kroupa & Tout (1997). We note that it is clear that the models are still not perfectly accurate, because the model color-magnitude relation falls blueward for the data for the faintest stars.

Since uncertainties about the quality of the theoretical mass-luminosity function remain, we also consider the use of an empirical mass-luminosity relation. This is available only for the solar neighborhood, and, consequently, only for stars of near solar composition. However, the median metallicity observed in the bulge may actually be quite similar to that of the solar neighborhood (McWilliam & Rich 1994), although the bulge metallicity distribution has a tail which extends to lower metallicities. Consequently, it is plausible that an empirical mass-luminosity relation derived from solar neighborhood stars will provide a reasonable match for the bulge. Such empirical relations have been presented by Henry & McCarthy (1993) and Kroupa et al. (1993), and the two show good agreement. However, the Henry and McCarthy relation is presented as a series of quadratic fits in different mass ranges. As a result, the derivative of their function, which enters into the derivation of a mass function from a luminosity function, is not continuous between the different regions which they fit, leading to problems with its use. Consequently, we adopt the Kroupa et al. function as our empirical function. This function has been tabulated for both the V and I passbands (among others) for stars with $M \leq 0.65$ by Kroupa & Tout (1997). For larger masses, the relation is given by Kroupa et al. (1993), but only for the V bandpass.

To get the I band mass-luminosity relation, we have transformed the V band mass-luminosity relation to the I band using a fit to color-magnitude data for solar neighborhood stars which was kindly provided by I.N. Reid; these data include ground-based measurements as well as those from the Hipparcos satellite. The applicability of this relation to the bulge stars can be judged by the degree to which the color-magnitude diagram of the bulge matches that of solar neighborhood stars. Figure 6 shows the median locus of the bulge stars compared with the solar neighborhood fit. One can see that these agree fairly well, though not perfectly. Minor differences may arise from different metallicity distributions between the bulge and the solar neighborhood, different fractions of binary systems in the samples, and errors in our assumed distance and/or extinction. Figure 6 also shows a solar metallicity model color-magnitude relation; this demonstrates the problems the models have getting the correct colors for the fainter stars.

Because neither the model nor the empirical mass-luminosity-color relations match the observed properties of the bulge stars perfectly, slightly different inferences are made about the mass function depending on whether the V or the I band luminosity function is considered.

3.4. The IMF

One can naively derive a MF from the luminosity function simply by using the M-L relation to effect a change of variables. However, this method has no way of accounting for systematic or random errors in the photometry which may be important for the fainter stars; it also cannot account for the presence of binary stars or spread in the distance to the stars. Of these different effects, the presence of binaries is the most significant, especially for the low-mass stars considered here. The effects of binaries have been previously discussed by Kroupa (1995) and Kroupa, Tout, & Gilmore (1993). Some of these effects are shown in Figure 7, which plots expected luminosity functions for the *same* initial mass function using our estimated completeness and several different assumptions about the presence of binaries and systematic errors. In this figure and hereafter, the binary fraction refers to the number of *systems* which are binaries. Also, we make the assumption that the masses of stars in binary systems are drawn independently from the same mass function. In Figure 7, the luminosity functions have been normalized to match at the bright end to make the differences in slope at the faint end most apparent. One can see that the presence of binaries can have a severe effect on the observed luminosity function. Depending on the mass function slope, this can dominate over the relatively small effects that random and systematic errors have on the luminosity functions, even for the faintest stars.

In the solar neighborhood, various studies suggest that the binary fraction is in the vicinity of 0.5 (see discussion in Kroupa 1995 and Kroupa et al. 1993). Of course, we have no idea whether the bulge binary fraction is similar to that of the solar neighborhood, so we consider it to be a free parameter.

To account for the presence of binaries and errors, a derivation of an IMF involves simulating a luminosity function from some assumed mass function, allowing for systematic errors, binaries, and distance spread, and then checking for consistency with the observed luminosity function. To do this, however, requires some parameterization of the mass function in order to keep the number of possible models reasonably small. Here, we initially transform our luminosity function into a mass function ignoring binaries and errors in order to determine what might provide a useful parameterization, and then simulate luminosity functions with binaries and errors for a more sophisticated comparison with model IMFs.

3.4.1. No binaries or errors

Figure 8 presents mass functions derived using both the F814W (top) and the F555W (bottom) luminosity functions; results using the F555W are more uncertain because the F555W data have larger photometric errors and less accurate completeness estimates. The inferred mass functions are shown using the empirical mass-luminosity relation (squares), a solar metallicity model mass-luminosity relation (triangles), and a model mass-luminosity relation for a population with $Z=0.006$ ($[\text{Fe}/\text{H}] \sim -0.5$). For one of the relations (triangles), solid points show completeness-corrected data and open points show raw data, to illustrate the amplitude of the completeness corrections.

Independent of the choice of mass-luminosity relation, no single power law mass function is able to fit the data; the derived mass-function shows a break around $0.5\text{-}0.7 M_{\odot}$. This conclusion depends on having a reasonable estimate of the completeness, since the turnover occurs at a level where our data are only $\sim 50\%$ complete. However, our completeness estimate would have to be off by a factor of two for stars of $0.4 M_{\odot}$ to be consistent with a single power-law mass function. As discussed in §2.2, we do not believe this is likely.

For masses less than $\sim 0.7 M_{\odot}$, evolution is negligible, so this result implies that the *initial* mass function cannot be fit with a single power law. A similar result is derived for the solar neighborhood by Kroupa et al. (1993) and by Gould et al. (1997). Both of these studies find a mass function slope of $\alpha = -2.2$ for stars with $M > 0.5 M_{\odot}$. For lower mass stars, Kroupa et al. find a slope of $-1.85 < \alpha < -0.7$, and Gould et al. find $\alpha = -0.56$. Lines in Figure 8 are shown which correspond to $\alpha = -2.2$ and $\alpha = -0.56$. The data appear to be matched by a mass function with a faint end slope of $\alpha > -1$.

The more massive stars are reasonably well matched by $\alpha = -2.2$ for $M \gtrsim 0.7 M_{\odot}$ using the model mass-luminosity relation. The empirical mass-luminosity relation suggests a steeper slope for the most massive stars, but since evolutionary effects are significant for these stars, the empirical mass-luminosity relation is likely not applicable since the mean age of bulge stars is larger than that of solar neighborhood stars.

3.4.2. The effect of binaries and errors

As mentioned above, an accurate mass function cannot be derived by simply converting luminosities to masses because of the presence of binaries, systematic errors, and distance spread. Here we derive some model luminosity functions assuming mass functions with power law segments, motivated by the estimates provided by Figure 8.

The calculation of these models is complicated because of the observational incompleteness. In principle, one should be able to take the model magnitudes from a mass-luminosity relation, derive observed magnitudes using a distance and extinction estimate, and use the completeness estimate at that magnitude to predict an observed number of stars. In practice, however, this leads to problems because any errors in the mass-luminosity relation lead to large errors in the completeness corrections. As mentioned above, it is clear that such errors exist because neither the stellar model nor the empirical mass-luminosity relations are able to match the observations simultaneously in both bandpasses. The differences in the completeness correction which one derives from using the two different bandpasses to compute completeness can be severe. To avoid this problem, we compute model luminosity functions without accounting for incompleteness in the model, and compare these with the *completeness-corrected* data. In this section, we only show comparisons with the F814W luminosity function, which has the better determined completeness.

Figure 9 shows the observed luminosity function with calculated luminosity functions assuming $\alpha = -2.2$ for $M > 0.5 M_{\odot}$ and $\alpha = -0.5, -0.9, -1.3, -1.7$ for $M < 0.5 M_{\odot}$. These cover the possible ranges of solar neighborhood mass functions inferred by Kroupa et al. (1993). We also include a mass function with a constant power law slope $\alpha = -2.0$ (steepest curve). Results from both a solar metallicity model and an empirical mass-luminosity relation are shown (left and right), as well as results for three different binary fractions, where the binary fraction gives the number of systems which are binary.

The top panels show results for no binaries, the middle panels for 50% binaries and the bottom panels for 90% binaries, where binaries are assumed to have uncorrelated masses. As noted above, binaries have a strong influence on the luminosity function of faint stars. The models with no binaries seriously overestimate the number of faint stars, unless the faint-end slope flattens significantly at $M_{F814W} \sim 6.5$, corresponding to $\sim 0.7 M_{\odot}$. With binaries, the models provide a better match, although all models shown here are statistically significantly different from the observed data. Including binaries allows a steeper faint-end slope, but models with a constant slope at $\alpha \lesssim -2$ are inconsistent with the data.

The left panels use the model mass-luminosity relation taken from the solar metallicity models of Baraffe et al. (1997), while the right panels use the empirical relation tabulated in Kroupa & Tout (1997), combined with the relation presented in Kroupa et al. (1993) for brighter stars. The empirical mass-luminosity relation produces a dip in the luminosity function around $M_{F814W} \sim 6$ which is not apparent in the bulge data. Despite the differences between the empirical relation and the the model relation, the same general conclusions can be drawn; the slope of the mass function at low masses must be significantly

shallower than at higher masses.

We did many additional experiments to find models which match the data to within statistical uncertainties, and we found we had to go to models with several different power law segments to find acceptable fits. Finding a best fit with many free parameters does not strike us as providing significant physical insight, particularly given the uncertainties in the binary fraction, the mass-luminosity relation, and possible errors in our completeness correction. We choose here to show just several plausible mass functions which match the observed luminosity function. Figure 10 shows one luminosity function derived using a mass function which has $\alpha = -2.2$ for $M > 0.7 M_{\odot}$, $\alpha = -0.9$ for $M < 0.7 M_{\odot}$, a solar metallicity model, and a binary fraction of 0.0, and another with a binary fraction of 0.5 and mass function slopes of $\alpha = -2.2$ for $M > 0.7 M_{\odot}$, $\alpha = -1.3$ for $M < 0.7 M_{\odot}$.

If one compares the model luminosity functions with the F555W data (which may have less well determined completeness corrections), one reaches similar conclusions; in fact, an even shallower faint-end slope is required to match these data.

4. Summary

We have measured a deep luminosity function in the Galactic bulge, and used it to infer a mass function. We find that the luminosity function down to $M_I \sim 9$ is similar to that observed in the solar neighborhood. Transforming the luminosity function into a mass function, we find strong evidence of a break from a power law mass function around $0.5 - 0.7 M_{\odot}$. Detailed modelling of a population allowing for binaries and photometric errors as inferred from our data suggests a mass function which flattens from a slope of $\alpha = -2.2$ for $M > 0.7 M_{\odot}$ to $\alpha \sim -1$ for $M < 0.7 M_{\odot}$. The exact details of the derived mass function depend on assumptions about the binary fraction, the mass-luminosity relation, and the details of our completeness corrections.

The similarity of the mass function in the bulge to that of the solar neighborhood is perhaps not surprising given that the mean metallicities of the two populations may not differ by a large amount (McWilliam & Rich 1994). The current data suggest that the physical processes of star formation in the bulge and in the disk may be similar.

Additionally, the lack of large numbers of low mass stars in the bulge may lead to difficulties in explaining the relatively high optical depth in microlensing events and the large number of short duration events observed in the direction of the bulge. Models that account for these with a population of stars require a stellar mass function with $\alpha \sim -2$ all the way down to the hydrogen-burning limit (Zhao, Spergel, & Rich 1995; Han & Gould

1996). Model luminosity functions for this slope are shown as the steepest curves in Figure 9. If one were to normalize these curves to the bright end of the luminosity function, one can see that the observed star counts at the fainter magnitudes fall significantly short of those expected for this mass function.

We can estimate the mass surface density observed towards Baade’s Window using the models which do a reasonable job of fitting the observed luminosity function (Figure 10). We compute surface mass densities towards Baade’s window for our assumed distance of 8 kpc, using several different assumptions about the lower mass cutoff of objects. For the model with no binaries and $\alpha = -0.9$ at the low mass end, we derive mass densities of 1.0, 1.3, & $1.4 \times 10^3 M_{\odot}\text{pc}^{-2}$ for lower mass cutoffs of 0.3, 0.08, and $0 M_{\odot}$. For the model with 50% binaries and $\alpha = -1.3$ at the low mass end, we derive mass densities of 1.1, 1.7, & $2.1 \times 10^3 M_{\odot}\text{pc}^{-2}$. If we assume that the entire bulge has a similar mass function, we can derive a total bulge mass by scaling these numbers by the ratio of the integrated infrared light from the bulge to that from Baade’s Window (c.f. Han 1997). For the range of mass densities above, we derive a total bulge mass of somewhere between 7.4×10^9 and $1.5 \times 10^{10} M_{\odot}$.

This work was supported in part by NASA under contract NAS7-918 to JPL. We gratefully acknowledge I. Baraffe and F. Allard for communicating some of their stellar model and atmosphere results before publication. We thank the referee, A. Gould, for several very useful comments and suggestions.

REFERENCES

- Alcock, C., Allsman, R.A., Alves, D., Axelrod, T.S., Bennett, D.P., Cook, K.H., Freeman, K.C., Griest, K., Guern, J., Lehner, M., Marshall, S., Park, H.-S., Perlmutter, S., Peterson, B.A., Pratt, M.R., Quinn, P. J., Rodgers, A. W., Stubbs, C. W., & Sutherland, W., 1997, *ApJ* 479, 119
- Alcock, C., Allsman, R.A., Alves, D.R., Axelrod, T.S., Becker, A.C., Bennett, D.P., Cook, K.H., Freeman, K.C., Griest, K., Gould, A., Guern, J.A., Lehner, M.J., Marshall, S.L., Minniti, D., Peterson, B.A., Popowski, P., Pratt, M.R., Quinn, P.J., Rodgers, A.W., Stubbs, C.W., Sutherland, W., Vandehei, T., Welch, D.L., 1998, *ApJ* 493, in press
- Allard, F., Hauschildt, P.H., Alexander, D.R., Starrfield, S., 1997, *ARAA* 35, 137
- Baraffe, I., Chabrier, G., Allard, F., & Hauschildt, P.H., 1997, *A&A* 327, 1054
- Bertelli, G., Bressan, A., Chiosi, C., Fagotto, F., & Nasi, E., 1994, *AAS*, 106, 275
- Bressan, A., Fagotto, F., Bertelli, G., Chiosi, C., 1993, *AAS* 100, 647
- Carney, B., Fulbright, J. P., Terndrup, D.M., Suntzeff, N. Walker, A., 1995, *AJ* 110, 1674
- Dahn, C., Lieber, J., Harris, H, & Guetter, H.C., 1995, in *An ESO Workshop on: The Bottom of the Main Sequence and Beyond*, ed. C.G. Tinney (Berlin, Springer)
- De Marchi, G. & Paresce, F., 1995a, *AA* 304, 202
- De Marchi, G. & Paresce, F., 1995b, *AA* 304, 211
- De Marchi, G. & Paresce, F., 1997, *ApJ* 476, L19
- Fagotto, F., Bressan, A., Bertelli, G., & Chiosi, C., 1994a, *AAS*, 104, 365
- Fagotto, F., Bressan, A., Bertelli, G., & Chiosi, C., 1994b, *AAS*, 105, 29
- Gould, A., Bahcall, J.N., & Flynn, C., 1997, *ApJ* 482, 913
- Gould, A., Popowski, P., & Terndrup, D.M. 1998, *ApJ*, 492, in press
- Gould, A., Flynn C., & Bahcall, J.N., 1997, *astro-ph* 9711263
- Grillmair, C.J, Mould, J.R., Holtzman, J.A., Worthey, G.S., et al., *ApJ*, in press
- Han, C., 1997, *ApJ* 484, 555
- Han, C. & Gould, A., 1996, *ApJ* 467, 540
- Henry, T.J. & McCarthy, D.W, 1993, *AJ*, 106, 773
- Holtzman, J.A., Light, R.M., Baum, W.A., Worthey, G., Faber, S.M., Hunter, D.A., O’Neil, E.J., Kreidl, T.J., Groth, E.J., and Westphal, J.A., 1993, *AJ*, 106, 1826

- Holtzman, J. A., Hester, J. J., Casertano, S., Trauger, J. T., Watson, A. M., et al. 1995a, *PASP*, 107, 156 (H95A)
- Holtzman, J. A., Burrows, C. J., Casertano, S., Hester, J.J., Trauger, J.T., Watson, A. M., & Worthy, G., 1995b, *PASP*, 107, 1065 (H95B)
- Holtzman, J.A., Mould, J.R., Gallagher, J.S., Watson, A.M & the WFPC2 IDT, 1997, *AJ* 113, 656
- Hunter, D.A., Light, R.M., Holtzman, J. A., Lynds, R., O’Neil Jr., E.J., & Grillmair, C.J., 1997, *AJ* 478, 124
- Kroupa, P., Tout, C. A., & Gilmore, G. 1993, *MNRAS*, 262, 545
- Kroupa, P. 1995, *ApJ*, 453, 358
- Kroupa, P. & Tout, C. A., 1997, *MNRAS*, 287, 402
- McWilliam, A. & Rich, R.M., 1994, *ApJS* 91, 749
- Miller, G.E. & Scalo, J.M., 1979, *ApJS*, 41, 513
- Monet, D.G, Dahn, C.C., Vrba, F.J., Harris, H.C., Pier, J.R., Luginbuhl, C.B., & Ables, H.D., 1992, *AJ*, 103, 638
- Mould, J. R., 1996, *PASP* 108, 35
- Richer, H.B. & Fahlman, G.G. 1992, *Nature* 358, 383
- Richer, H.B., Fahlman, G.G., Buononno, R., Fusi Pecci, F., Searle, L., & Thompson, I.B., 1991, *ApJ* 381, 147
- Salpeter, E.E., 1955, *ApJ* 121, 161
- Stanek, K.Z., 1996, *ApJ* 460, L37
- Wielen, R., Jahreiss, H., & Kruger, R., 1983, in *Nearby Stars and the Stellar Luminosity Function*, IAU Colloquium 76, eds. A.G. Davis Phillip & A.R. Uppgren (Schenectady: L. Davis Press), p. 163
- Zhao, H., Spergel, D.N., & Rich, R.M., 1995, *ApJL* 440, L13

Fig. 1.— The WFPC2 F814W image of the Baade's window field.

Fig. 2.— The observed WFPC2 color-magnitude diagram. The different panels have F555W and F814W on the ordinate. Only one in every four stars is plotted.

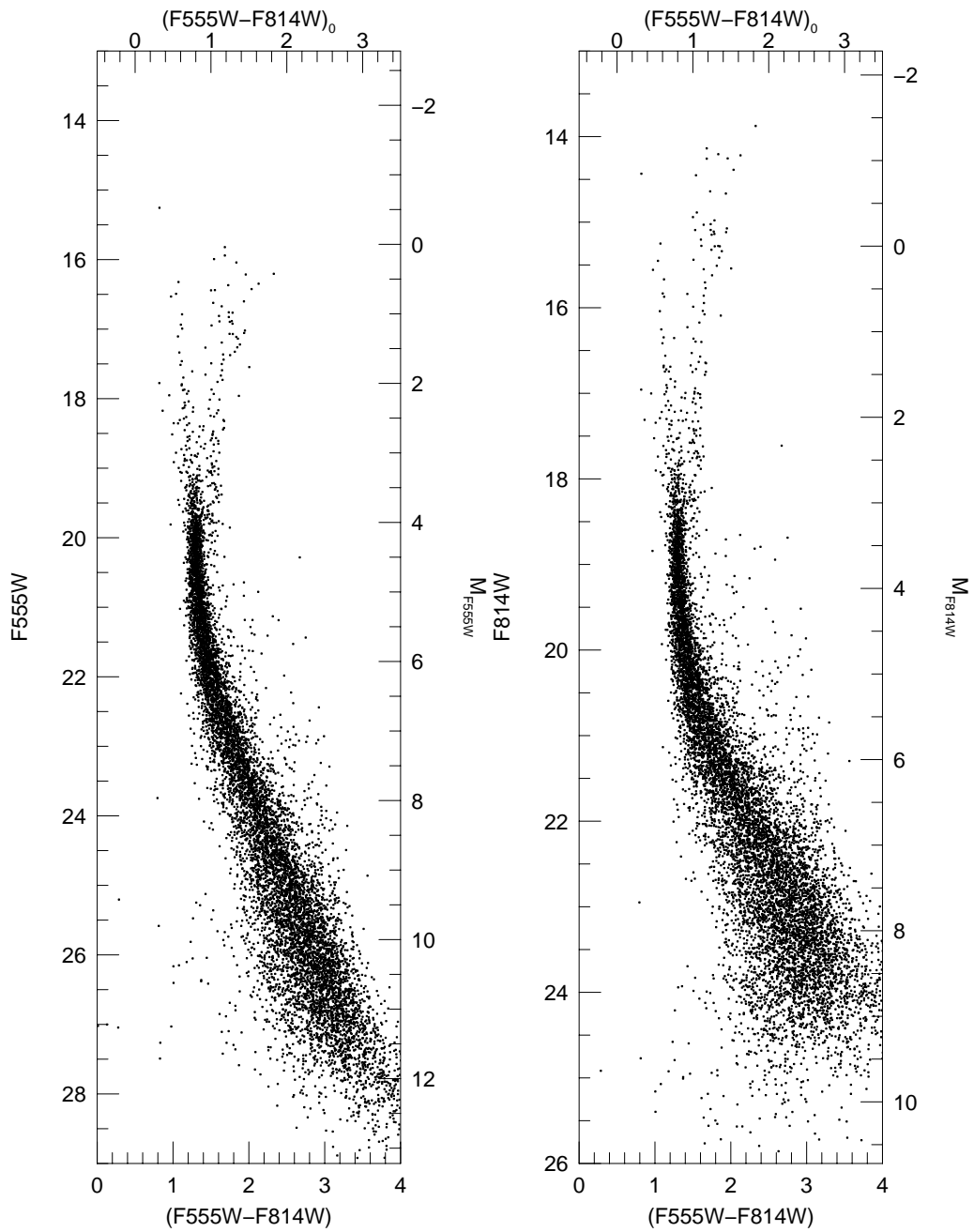


Fig. 3.— Completeness and error distributions. Each panel shows the actual errors in F814W for simulated stars at a brightness which is given in the upper right. The fraction of stars found at each brightness is also noted.

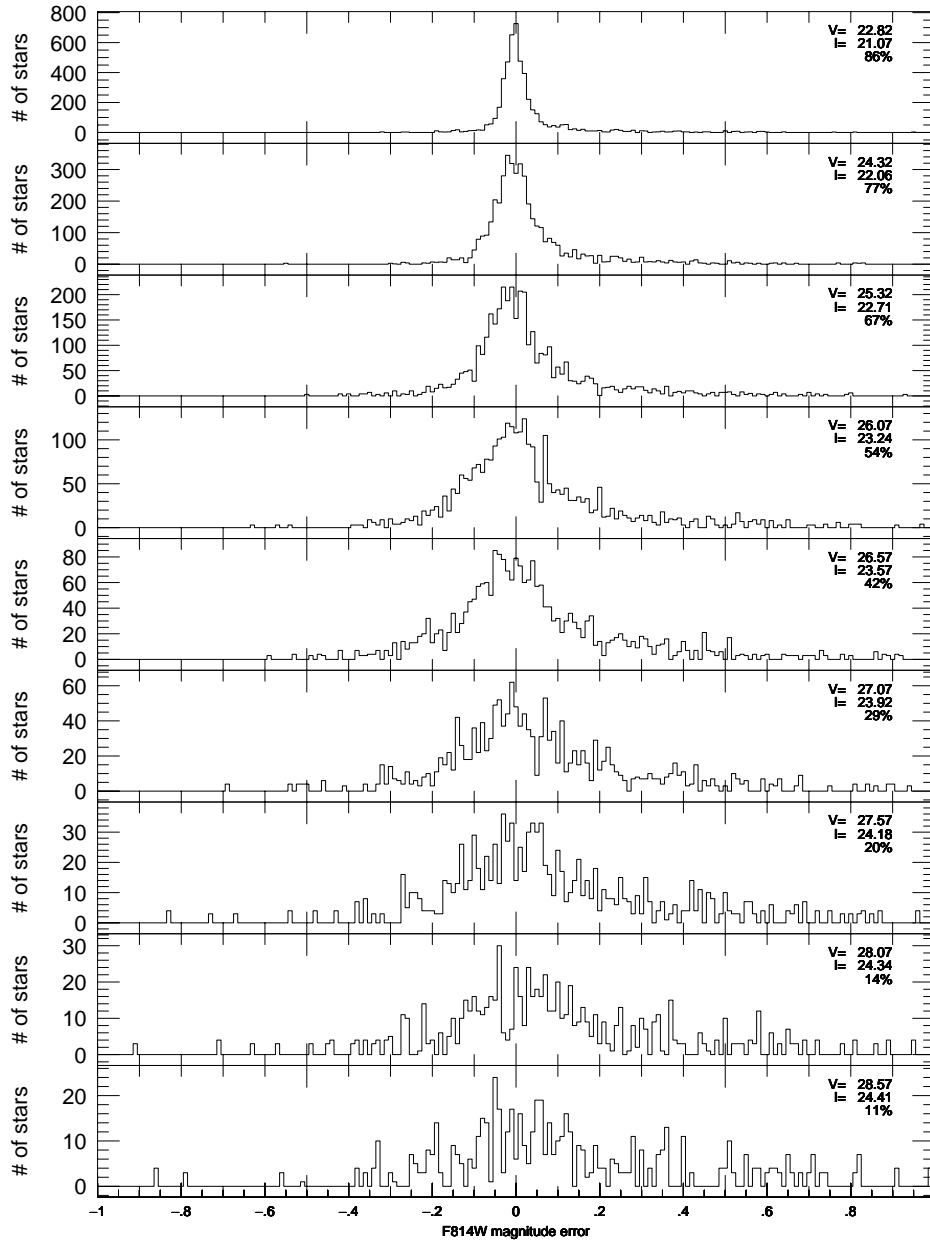


Fig. 4.— Completeness corrections, as derived from simulated stars. The solid curve gives the correction inferred for PSFs derived to match the actual data. The dotted curve gives the result if a different PSF is used to create the simulated stars from that used to reduce them, where the erroneous PSF for this case represents an extreme mismatch.

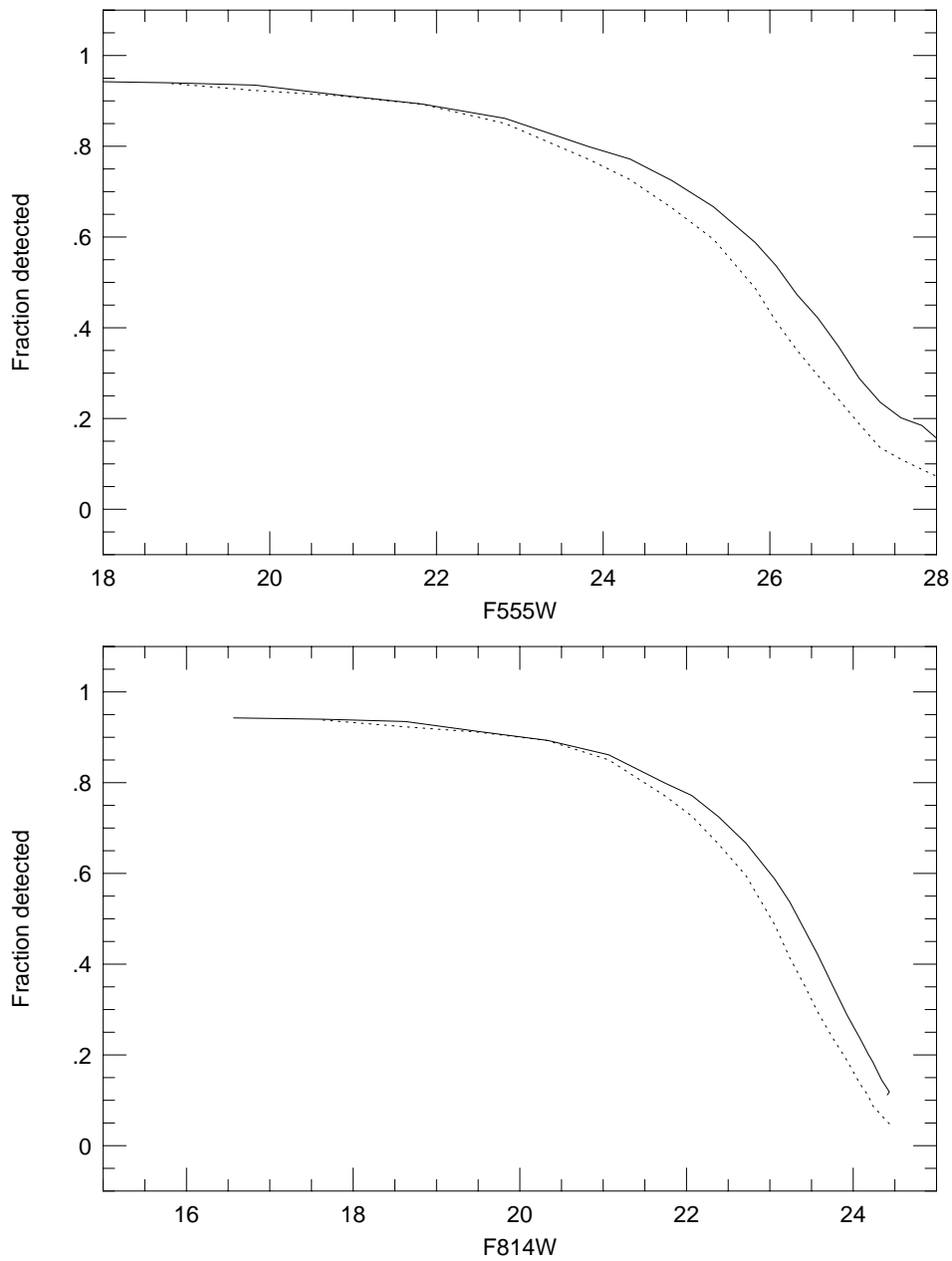


Fig. 5.— The observed WFPC2 luminosity functions, in F555W (top) and F814W (bottom). The raw luminosity function is shown with open squares, while a completeness-corrected function (without correction for systematic errors) is shown with filled squares. Data have been normalized to number of stars per square arcmin per magnitude. Triangles show the solar neighborhood luminosity function of Wielen et al. (1983), and asterisks show that derived by Gould et al. (1997)

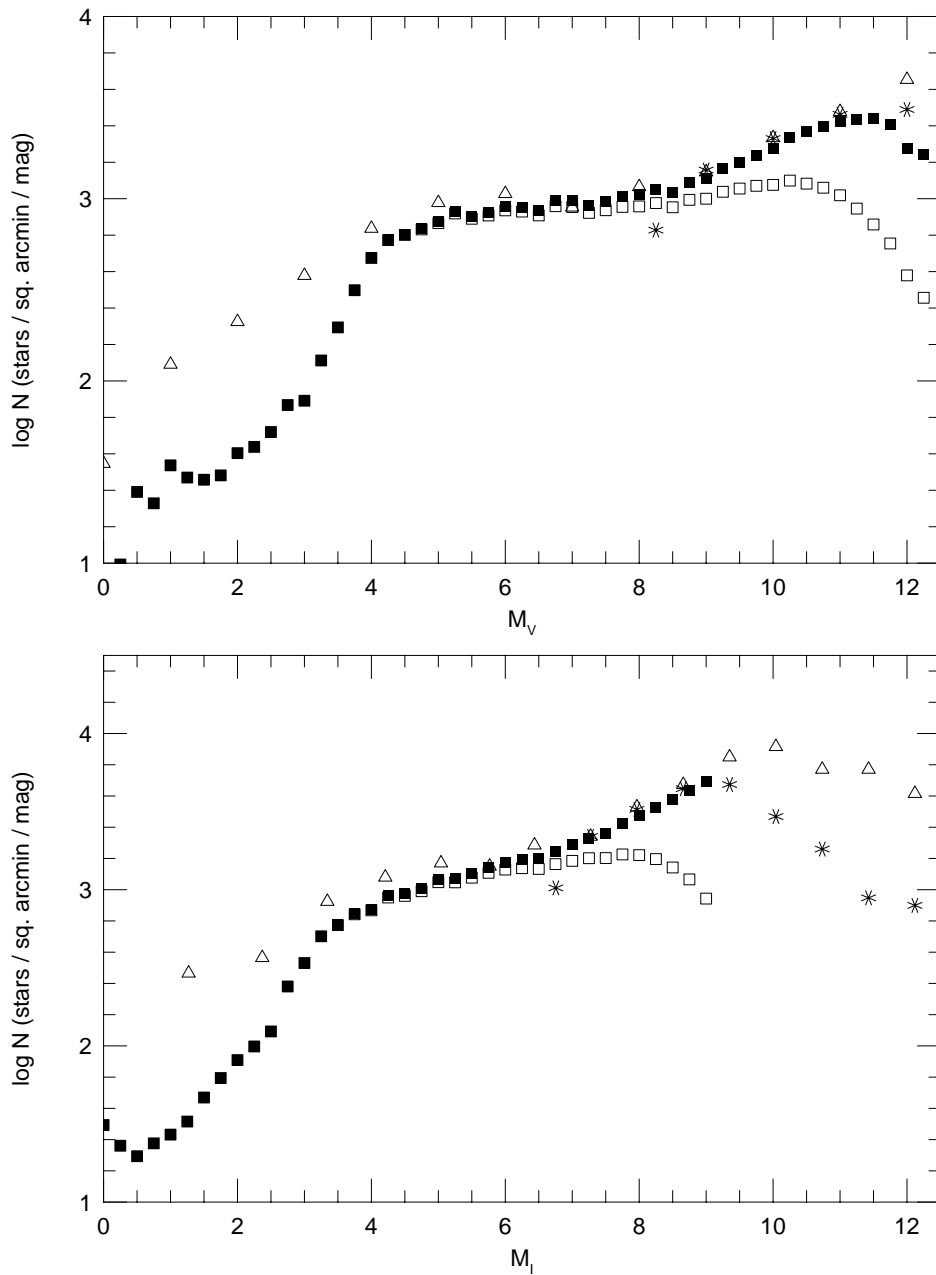


Fig. 6.— The mean locus of the bulge data in a color-magnitude diagram (points) along with a fit to color-magnitude data of solar neighborhood stars (solid line), and a model color-magnitude relation (dotted line).

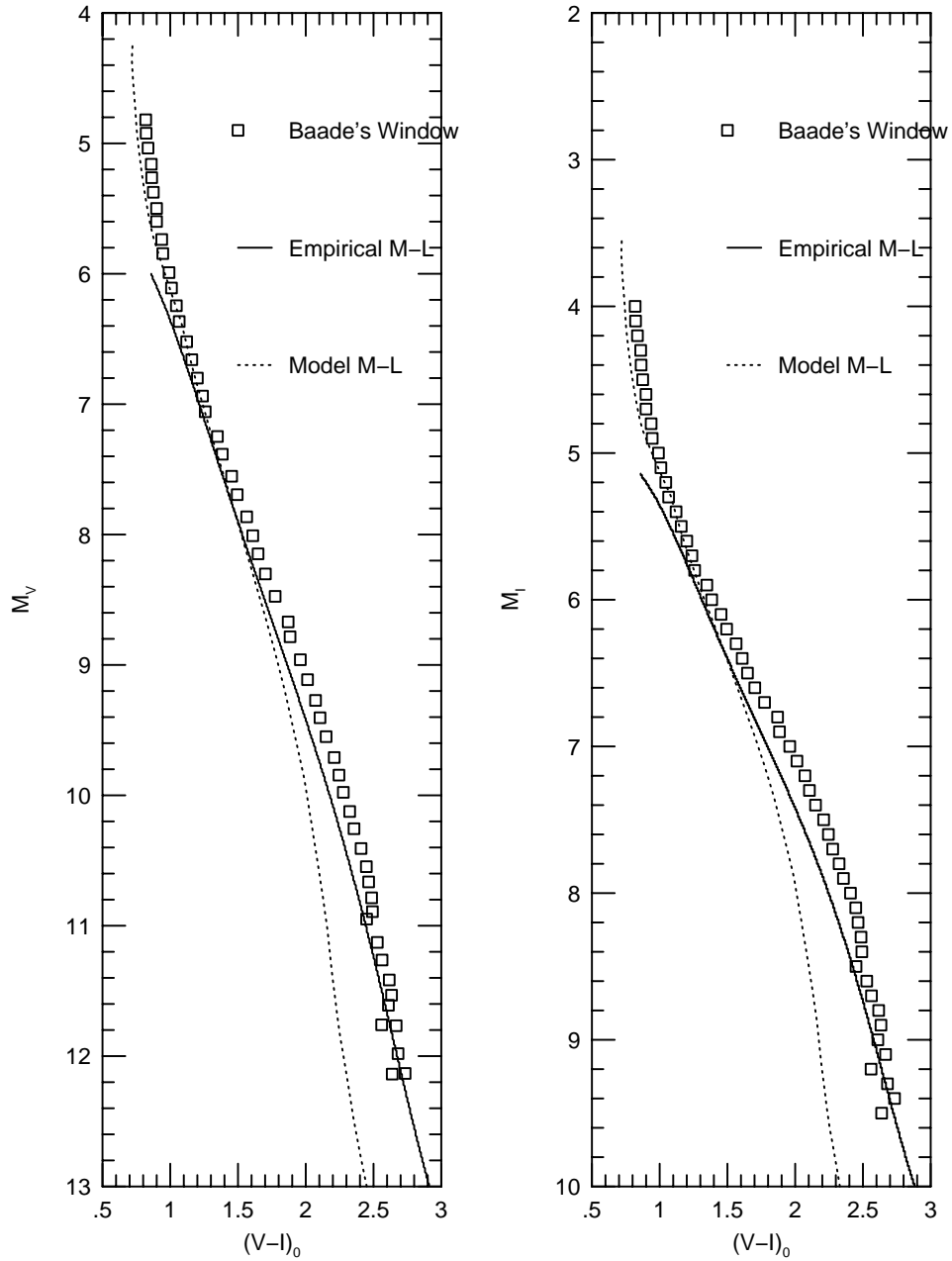


Fig. 7.— Some simulated model luminosity functions to illustrate the effect of errors and the presence of binaries. All luminosity functions shown here were created using the same initial mass function, with $\alpha = -2.2$ for $M > 0.5M_{\odot}$, $\alpha = -0.5$ for $M < 0.5M_{\odot}$.

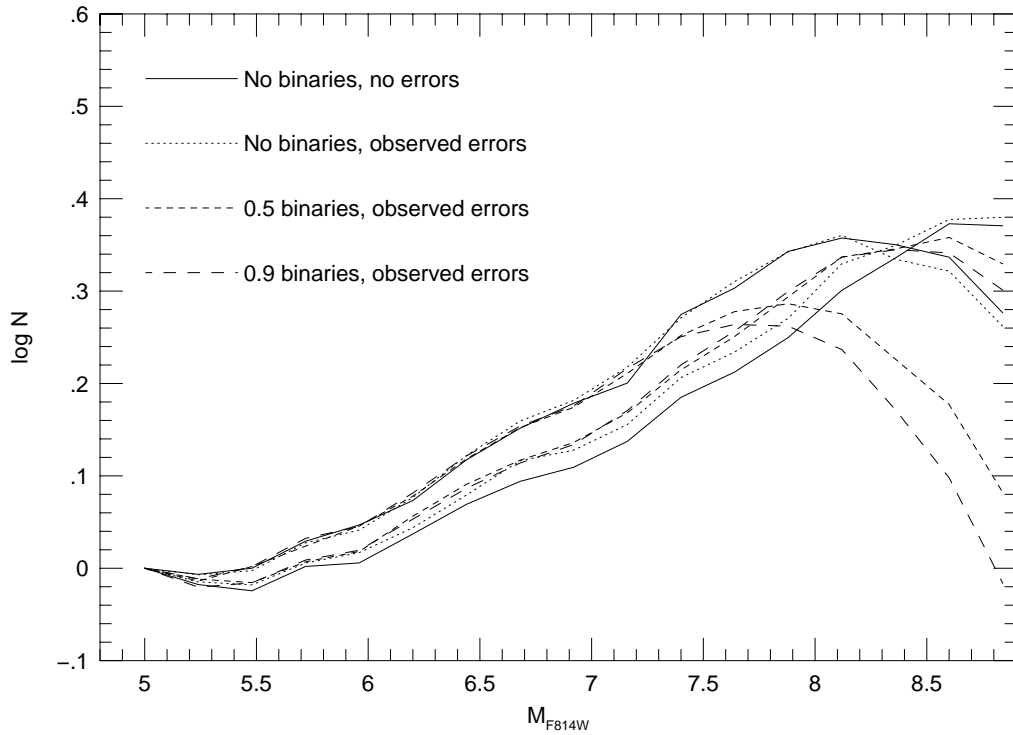


Fig. 8.— Inferred mass functions from F814W luminosity function (top) and F555W luminosity function (bottom) without correction for binaries or systematic errors. Results using three different mass-luminosity relations are shown: solar-metallicity models (triangles), lower-metallicity models (circles), and empirical mass-luminosity relation (squares). For the triangles, open symbols are for raw data, and filled symbols show the completeness-corrected counts. Lines above the data show slopes of $\alpha = -2.2$ and $\alpha = -0.56$.

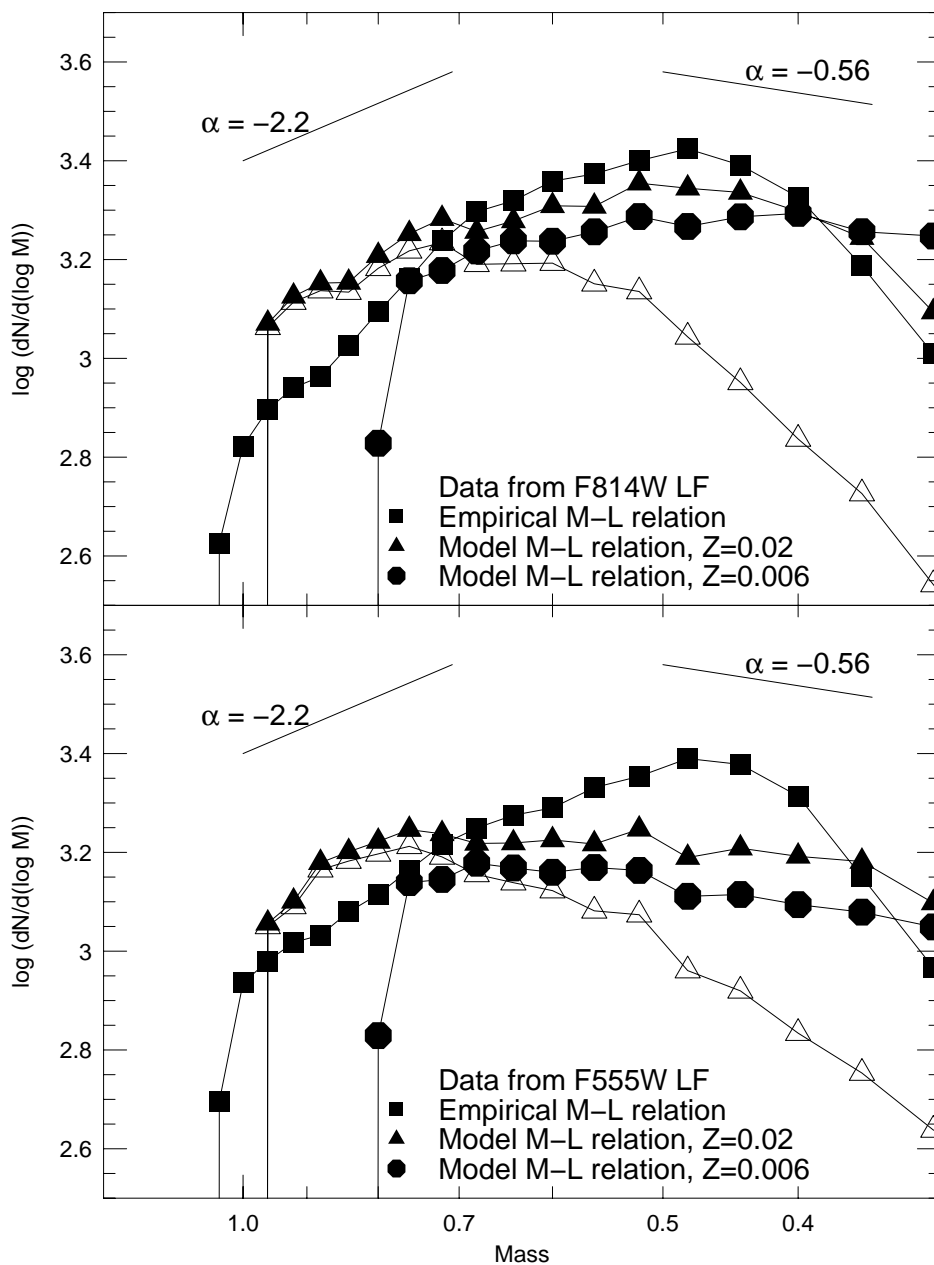


Fig. 9.— Some model F814W luminosity functions, along with the observed one (bold line). In each panel five models are shown. Four models have $\alpha = -2.2$ for $M > 0.5M_{\odot}$, but different lower-mass slopes, with $\alpha = -0.5, -0.9, -1.3,$ and -1.7 for $M < 0.5 M_{\odot}$. The fifth model (steepest) has a constant slope of $\alpha = -2.0$ over the entire mass range. Upper panels assume no binaries, middle panels have a binary fraction of 0.5, and lower panels have a binary fraction of 0.9. Left panels use a solar metallicity model mass-luminosity relation, while right panels use an empirical mass-luminosity relation.

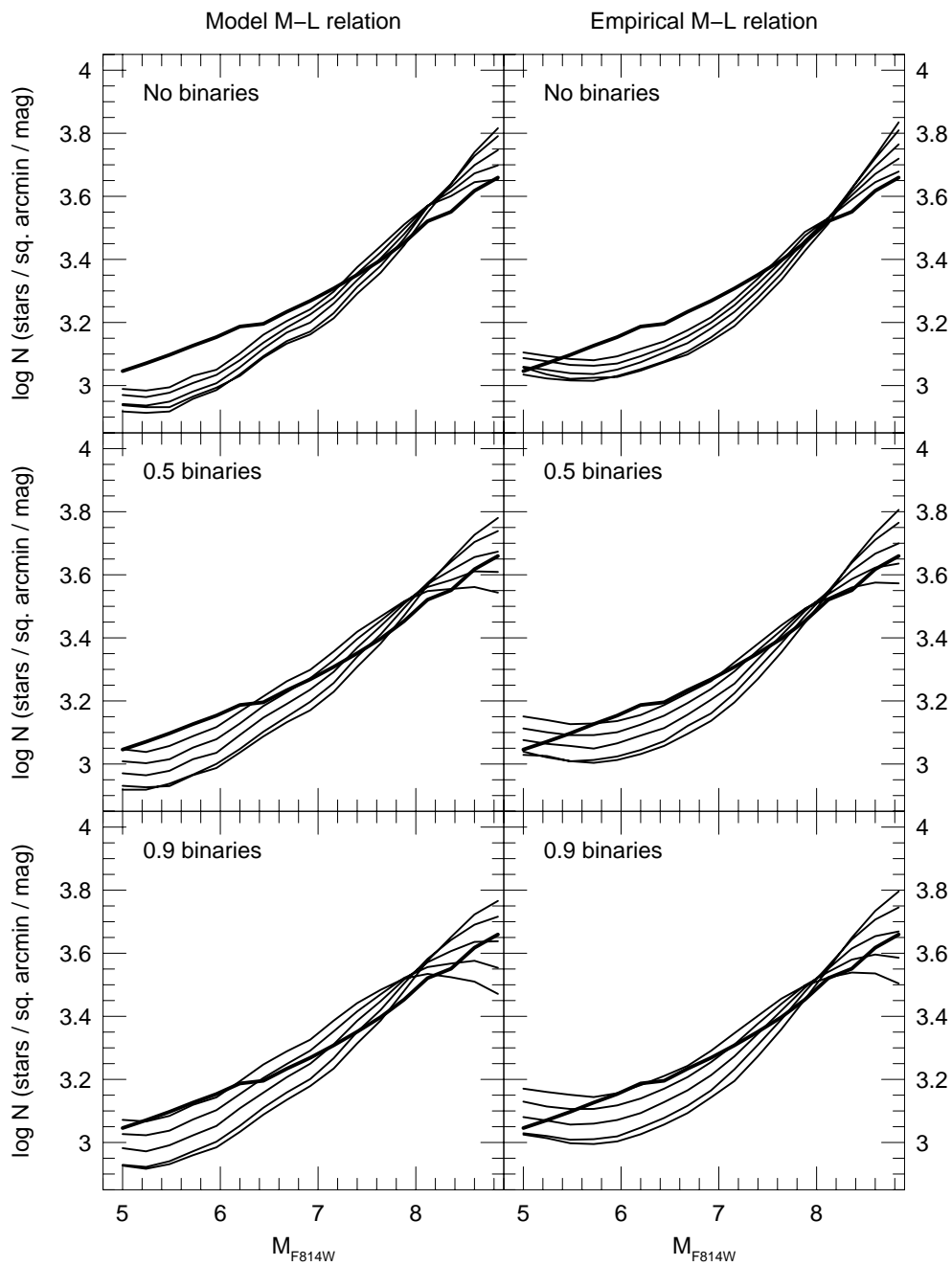


Fig. 10.— Two reasonable-fit model luminosity functions. These use 2 different power-law segments, with a break at $0.7 M_{\odot}$.

